International Journal of Fluid Machinery and Systems
Vol. 3, No. 2, April-June 2010

**Original Paper**

# Multi-objective Optimization of a Laidback Fan Shaped Film-Cooling Hole Using Evolutionary Algorithm

**Ki-Don Lee, Afzal Husain and Kwang-Yong Kim**

Department of Mechanical Engineering, Inha University
253 Yonghyun-Dong, Incheon, 402-751, Republic of Korea
leekd@inha.edu, afzal19@inha.ac.kr, kykim@inha.ac.kr

**Abstract**

Laidback fan shaped film-cooling hole is formulated numerically and optimized with the help of three-dimensional numerical analysis, surrogate methods, and the multi-objective evolutionary algorithm. As Pareto optimal front produces a set of optimal solutions, the trends of objective functions with design variables are predicted by hybrid multi-objective evolutionary algorithm. The problem is defined by four geometric design variables, the injection angle of the hole, the lateral expansion angle of the diffuser, the forward expansion angle of the hole, and the ratio of the length to the diameter of the hole, to maximize the film-cooling effectiveness compromising with the aerodynamic loss. The objective function values are numerically evaluated through Reynolds- averaged Navier-Stokes analysis at the designs that are selected through the Latin hypercube sampling method. Using these numerical simulation results, the Response Surface Approximation model are constructed for each objective function and a hybrid multi-objective evolutionary algorithm is applied to obtain the Pareto optimal front. The clustered points from Pareto optimal front were evaluated by flow analysis. These designs give enhanced objective function values in comparison with the experimental designs.

**Keywords**: Film-cooling, Numerical analysis, Multi-objective optimization, Response Surface Approximation

## 1. Introduction

In the design of up-to-date gas turbine, the inlet temperature of the turbine stage has been continuously increased to achieve high thermal efficiency and specific thrust. Therefore, the development of effective cooling technique is recognized as an essential part in the gas turbine research. Among many others, film-cooling technique [1] has been widely used for gas turbine blades as the very important alternative. In this technique, coolant air is injected on the surface to provide a protective layer which helps in maintaining the external walls at an acceptable temperature level, thus protecting the turbine blade from failure. However, film-cooling inevitably results in increasing the aerodynamic loss due to the interaction of the mainstream hot gas with the coolant jet. In the design of the hole geometry, thus, the film-cooling effectiveness as well as the aerodynamic loss should be considered.

It is well known that significant improvement can be achieved in cooling performance of the film by using diffused exit shaped holes. Many experimental and numerical investigations have been performed for diffused exit shaped holes to analyze the cooling efficiency and the aerodynamic loss. Gritsch et al. [2] conducted an experimental investigation to determine the effects of hole geometry and crossflow Mach number on film cooling performance for a cylindrical hole and two holes with a diffuser-shaped exit portion. Saumweber and Schulz [3] investigated the effects of the expansion angle of the diffuser, the inclination angle of the hole, and the length of the cylindrical part at the entrance of fan-shaped and cylindrical holes. Saumweber et al. [4] studied the variation of the film-cooling performance with the turbulence intensity of the free-stream and the ejection angle for cylindrical and two different-shaped holes. From measurements on a range of the L/D ratio of 1.75 to 18, Lutum and Johnson [5] reported that film-cooling effectiveness generally decreased with decreasing L/D when the ratio was less than 5.0 but showed no significant change for L/D that exceeded 5.0. Bunker [6] examined the origins of the shaped film-cooling hole and summarized the extensive literature regarding the performance of such film holes. In order to evaluate the performance and characteristics of various hole-shapes, many numerical studies have been conducted, e.g., Bohn and Moritz [7], Hyams and Leylek [8], Azzi and Jubran [9], Leedom and Acharya [10] and Mahmood et al. [11]. Day et al. [12] presented a method to define the aerodynamic loss for a film-cooled annular cascade, and a simple mixing model was suggested to analyze the loss contribution for the case of compressible flow and heterogeneous gases. Sargison et al. [13] reported the thermal and aerodynamic performance for the novel console hole

Received June 3 2010; revised June 6 2010; accepted for publication June 7 2010: Review conducted by Prof. Tadashi Tanuma. (Paper number O10012J)
Corresponding author: Mr. Ki-Don Lee, leekd@inha.edu

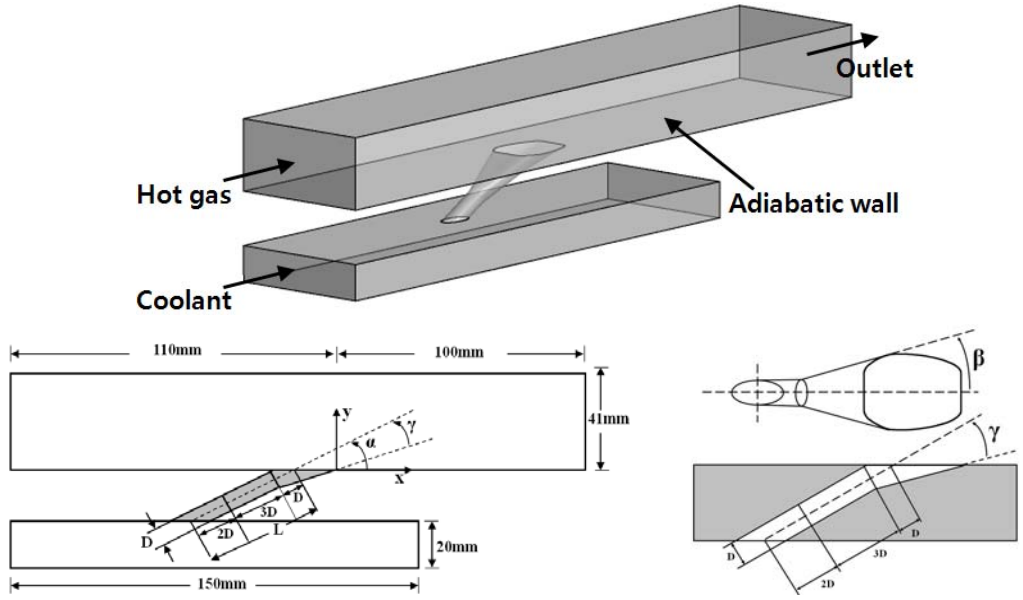


**Fig. 1** Computational domain and geometric parameters

and other conventional film cooling hole. Dibbon et al. [14] documented a numerical investigation of the aerodynamic impact of film cooling on a turbine airfoil cascade with single row injection hole. Their numerical results were compared to experimental data in terms of total pressure loss downstream of the blade row, and they reported that the computational methods can be used to predict losses accurately. And, as the study for optimization of film-cooling hole shape, Lee and Kim [15, 16] reported single objective optimization works using surrogate modeling for a cylindrical and fan-shaped film cooling hole. As mentioned above, the effects of various parameters on the film cooling effectiveness and the aerodynamic loss have been tested by many experimental and numerical works. However, design optimization simultaneously considering film-cooling effectiveness and aerodynamic loss has not been performed yet.

Practical engineering design generally involves multiple disciplines and simultaneous optimization of multiple objectives related to each discipline. These design problems usually known as multi-objective problems require simultaneous consideration of all objective functions to optimize the system. There are numbers of solution methods and algorithms available for solving multi-objective optimization problems [17]. A multi-objective optimization problem consists of many optimal solutions called Pareto-optimal solutions; therefore a designer's aim is to find as many optimal solutions within the design range as possible. This helps designer to find a global Pareto-optimal front. Each design set corresponding to optimal solution represents a compromise of design objectives. Elitist Non-dominated Sorting Genetic Algorithm (NSGA-II) combining with ε-constraint strategy of local search method is used for hybrid multi-objective evolutionary algorithm (hybrid MOEA) [17]. Review of multi-objective optimization methods for engineering was presented by Marler and Arora [18]. NSGA-II applications have been reported by Samad et al. [19] and Foli et al. [20], who applied multi-objective optimization approach using evolutionary algorithm to dimpled channel and micro heat exchanger optimizations, respectively. And, Samad and Kim [21] performed single- and multi-objective shape optimization for a compressor blade.

In the present study, a laidback fan shaped film-cooling hole has been numerically formulated using Reynolds-averaged Navier-Stokes (RANS) analysis, and the numerical results have been compared with the experimental data for the validation of present numerical simulation. And, shape optimization of a laidback fan shaped hole considering the film-cooling effectiveness and aerodynamic loss has been performed using hybrid evolutionary multi-objective algorithm (hybrid MOEA). A set of optimal designs are presented by Pareto optimal solutions. The trade-off between the two objective functions has been explored and discussed with respect to the design variables.

## 2. Numerical Analysis

To analyze fluid flow and film-cooling, three-dimensional Reynolds-averaged Navier-Stokes (RANS) analysis has been performed using ANSYS-CFX 11.0 [22] which employs unstructured grid system. The solutions are obtained by using finite volume method to discretize the RANS equations.

Fig. 1 shows the laidback fan-shaped hole geometry and geometric parameters. The computational domain is composed of a main channel of hot gas stream, a coolant channel, and a fan-shaped film cooling hole. Diameter of the cylindrical part of the hole (D) is 5 mm and width of the channel is 40 mm.

An important issue in the turbulence modeling is the treatment of near-wall turbulence. The near-wall formulation determines the accuracy of the wall shear stress. The shear stress transport (SST) turbulence model [23] is used as a turbulence closure. The SST model works by solving a turbulence/frequency-based model ($k$-$\omega$) near the wall and $k$-$\varepsilon$ model in the bulk flow. A blending function ensures a smooth transition between the two models. Bardina et al. [24] showed that the SST model more effectively captures flow separation under an adverse pressure gradient than other eddy viscosity models, and thus precisely predicts the near-wall turbulence that plays vital role in the prediction of turbulent heat transfer. An example of the unstructured hexahedral grid

**Table 1** Design variables and design space

| Design Variables | Lower bound | Upper bound |
|---|---|---|
| α (°) | 20 | 50 |
| β (°) | 12 | 24 |
| γ (°) | 0 | 20 |
| L/D | 5 | 8 |

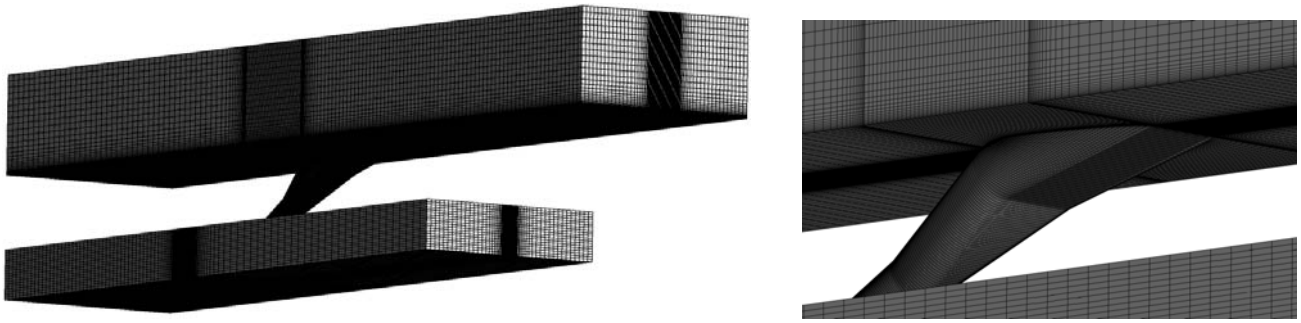

**Fig. 2** Example of computational grids

system used in this work is shown in Fig. 2. The grids are concentrated at the wall region to resolve the high velocity gradient. O-type grids are used in the hole. Near the wall, first grid points are placed at $y+$ less than 2 so that low-Re SST model can be implemented properly.

The working fluid is ideal gas (air). In terms of the boundary conditions, adiabatic and no-slip conditions are used at the walls, and constant mass flow rate at inlet of the cooling channel, total pressure at inlet of the main channel, and static pressure at outlet of the main channel are specified. In order to adjust Mach number of hot gas in the main channel to the experimental condition [4], 0.3, the total pressure at the inlet and the static pressure at the outlet are set to 100,400 Pa and 92,300 Pa, respectively. Temperatures of the hot gas and the coolant are 540 K and 310 K, respectively. Turbulence intensity in the main channel is 3.6 % and Reynolds number based on the hole diameter is 25,000.

RMS residual values of all flow parameters below 1.0E-5 and energy and mass imbalances in the entire computational domain less than 0.001% were employed as the convergence criteria. The solver finished a single simulation in approximately 1000 iterations, and the computations were performed by an Intel Quad Core 2.4 GHz PC. The computational time per a single simulation was typically 20~25 hours, and the time of computation depends on geometry considered.

## 3. Design Variables and Objective functions

For the optimization, four geometric variables, viz., the injection angle of the hole (α), the lateral expansion angle of the diffuser (β), the forward expansion angle of the hole (γ), and the ratio of the length to the diameter of the hole (L/D) are shown in Fig. 1. In the case of L/D, the length of the diffuser and the hole diameter are fixed, and only the length of the cylindrical part of the hole is varied. And the width of bottom side in the latter part of the cooling hole diffuser, where the forward angle (γ) is expanding, is kept constant. The design space is set as shown in Table 1. To determine the ranges of the design variables, preliminary calculations have been performed in wide ranges.

To maximize the performance of the film-cooling hole, two objective functions $F_{FCE}$ and $F_{AL}$ based on film-cooling effectiveness and aerodynamic loss, respectively, are selected. The main motive of the optimization is to minimize both of the objective functions, $F_{FCE}$ and $F_{AL}$.

$F_{FCE}$ is defined a reciprocal of spatially averaged film-cooling effectiveness which is averaged over an area of 6hole diameters in width and 20 hole diameters in the streamwise length.

$$F_{FCE} = 1/\eta_S \tag{1}$$

$$\eta_s = \frac{1}{6\times 20}\int_{-3}^{3}\int_{0}^{20}\eta(x/D, z/D)\,d(x/D)\,d(z/D) \tag{2}$$

$$\eta(x/D, z/D) = \frac{T_{aw}(x/D, z/D) - T_\infty}{T_c - T_\infty} \tag{3}$$

where $T_{aw}$ is local adiabatic wall temperature, and $T_\infty$ and $T_c$ are free-stream temperature in main channel and coolant jet temperature, respectively.

Another objective function, $F_{AL}$ is formulated as follows [12, 13]:

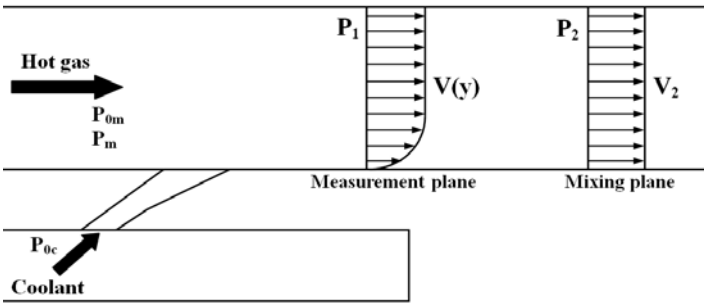


**Fig. 3** Measurement and mixing planes for aerodynamic loss

$$F_{AL} = 1 - \frac{KE_{Actual}}{KE_{Theoretical}} \tag{4}$$

$KE_{Actual}$ and $KE_{Theoretical}$ mean the actual and theoretical kinetic energy flux, respectively, at the mixing plane. The mixing plane is defined as the hypothetical plane at which the coolant and mainstream flows are fully mixed and the velocity, pressure and temperature are uniform. It is mathematically equivalent to the measurement plane and the velocity, static pressure and temperature at this plane are found by applying the laws of conservation of mass, momentum and energy between the measurement plane and the mixing plane [13]. Although this measurement is dependent on the dimensions of main channel, the purpose of the current measurement is to generate comparative data only.

Applying conservation of mass from the measurement plane to the mixing plane shown in Fig. 3,

$$v_2 = \frac{\iint_{A_m} v dy dz}{A_m} \tag{5}$$

Here, $A_m$ is the area of main channel. And, applying conservation of momentum,

$$P_2 = P_1 + \rho \iint_{A_m} v^2 dy dz - \rho A_m v_2^2 \tag{6}$$

From eq. (5) and (6), $KE_{Actual}$ can be calculated as follows:

$$KE_{Actual} = \frac{1}{2} \rho v_2^3 \tag{7}$$

The theoretical kinetic energy flux, $KE_{Theoretical}$, is calculated from the initial total pressure and static pressure at the mixing plane as follows:

$$KE_{Theoretical} = \frac{\dot{m}_m}{\rho_m}(P_{0m} - P_2) + \frac{\dot{m}_c}{\rho_c}(P_{0c} - P_2) \tag{8}$$

where $P_{0m}$ and $P_{0c}$ are total pressure of main channel and coolant plenum, respectively.

## 4. Optimization Methodology

### 4.1 Response Surface Approximation

Evolutionary algorithms require many evaluations for objective functions to search the optimum solutions. Therefore, to evaluate these objective function values, surrogate is constructed to avoid experimental or numerical expenses and to save time. In the present study, Response surface approximation (RSA) [25] surrogate method is applied to evaluate objective function values. RSA is a methodology of fitting a polynomial function for discrete responses obtained from numerical calculations. It signifies the association between response functions and design variables. For a set of $N$ design variables $x_j$, the linear response function is formulated as:

$$y_i = \sum_{j=1}^{N} \beta_j x_{ij} + \varepsilon_i \tag{9}$$

where errors, $\varepsilon_i$ are independently distributed and with zero mean and variance $\sigma^2$, i.e.,

$$E(\varepsilon_i) = 0 \text{ and } V(\varepsilon_i) = \sigma^2 \tag{10}$$

In the matrix form, equations (9) and (10) can be expressed as:

$$y = X\beta + \varepsilon \tag{11}$$

$$\mathrm{E}(\varepsilon) = 0 \text{ and } V(\varepsilon) = \sigma^2 I \tag{12}$$

where $y$ is a column matrix of $M$ responses and $X$ is an $M \times N$ matrix of design variable values. The least square estimate of $\beta$ is

$$\hat{\beta} = (X^T X)^{-1} X^T y \tag{13}$$

The constructed second order polynomial response can be expressed as:

$$y(x) = \beta_0 + \sum_{j=1}^{N} \beta_j x_j + \sum_{j=1}^{N} \beta_{jj} x_j^2 + \sum_{j=1}^{N} \beta_{ij} x_i x_j \tag{14}$$

For a second order polynomial model, used in the current study, the number of regression coefficients is *(N+1)×(N+2)/2*.

### 4.2 Multi-Objective Evolutionary Algorithm (MOEA)

A multi-objective optimization problem stated above is formulated as:

| | |
|---|---|
| Minimize | $\bar{f}(\bar{x})$ (M functions to be optimized) |
| Subject to | $\bar{g}(\bar{x}) \le 0$ (s inequality constraints) |
| | $\bar{h}(\bar{x}) = 0$ (t equality constraints) |

where $\bar{f}(\bar{x}) = \left\{\bar{f}_1(\bar{x}), \bar{f}_2(\bar{x}), \bar{f}_3(\bar{x}), \ldots\ldots \bar{f}_M(\bar{x})\right\}$ is a vector of $M$ real-valued objective functions, and $x$ is a vector of $N$ design variables. $\bar{x} \in R^N$, $\bar{g}(\bar{x}) \in R^s$, $\bar{h}(\bar{x}) \in R^t$. The present problem is associated with two competing objectives in which improvement of one objective leads to deterioration of other objective. Each feasible solution set $\bar{x}$ of multi-objective problem is either dominated or non-dominated, in which all non-dominated solutions are called Pareto optimal solutions. Vector $\bar{x}_i$ dominates a vector $\bar{x}_j$ if $\bar{x}_i$ is at least as good as $\bar{x}_j$ for all objectives and $\bar{x}_i$ is strictly better than $\bar{x}_j$ for at least one objective.

The methodology used to generate global Pareto optimal front (POF) is shown in Fig. 4. Objective functions are defined mathematically and evaluated on the data obtained by numerical simulation. A hybrid multi-objective evolutionary approach is used to obtain global Pareto optimal solutions. In this method, first, approximate Pareto optimal solutions are obtained using real

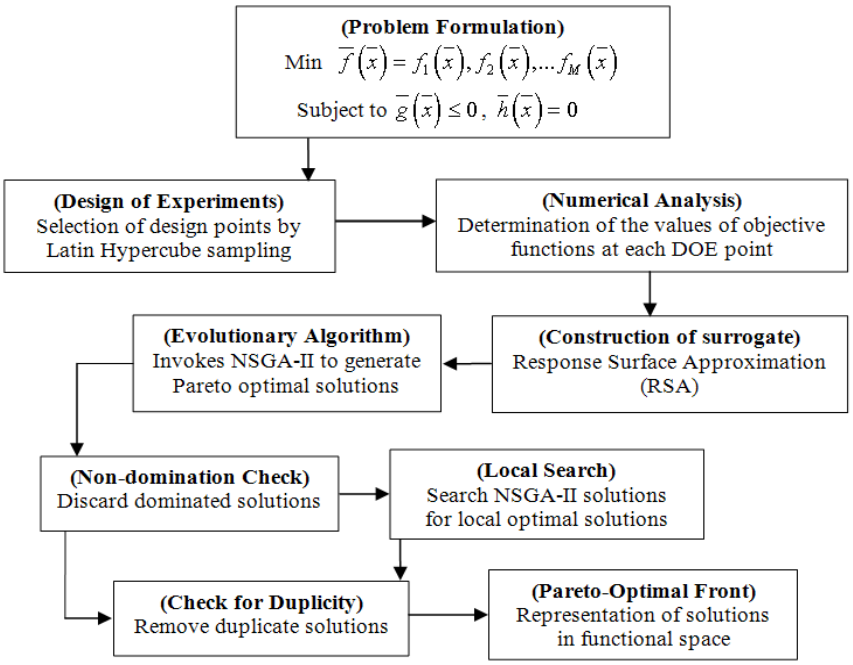


**Fig. 4** Multi-objective optimization procedure [19]

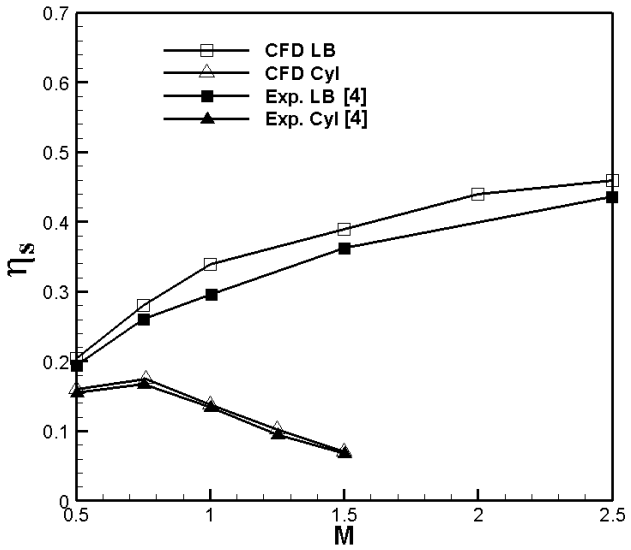


**Fig. 5** Validation of numerical results

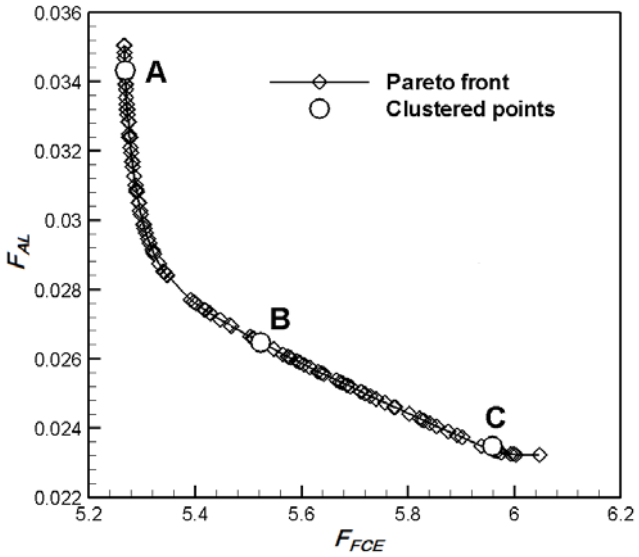


**Fig. 6** Pareto optimal solutions using hybrid MOEA

coded NSGA-II developed by Deb et al. [17] for two objective functions based on heat transfer and pressure drop. Here, real coded means that the crossover and mutations are conducted in real space to obtain a response of NSGA-II. These solutions are then refined by searching a local optimal solution for each objective function over the whole NSGA-II obtained optimal solutions using Sequential Quadratic Programming (SQP) [26] with NSGA-II solutions as initial guesses. SQP is a generalization of Newton's method which is gradient based optimization technique. To perform local search usually two approaches are applied [17]. In one approach all the objectives are combined into a single composite objective and optimum is searched. In another approach one objective is optimized treating the others as equality constraints and the process is repeated to all objectives. In the present study first objective is optimized and second objective is treated as equality constraint. The local search is repeated for second objective function treating the first as equality constraint. This process gives two new sets of optimal solutions which are then merged with the NSGA-II solutions. From these solutions, dominated solutions are discarded and then duplicate solutions are removed to get global Pareto optimal solutions. The process of local search improves the quality of Pareto optimal solutions.

## 5. Results and Discussion

Initially, to determine the optimum number of grid, grid dependency was evaluated by taking several different grid systems for the reference geometry, and approximately 1,800,000 were selected as optimum number of grids. At next step, the numerical results were validated with the experimental date presented by Saumweber et al. [4] for the same conditions. Fig. 5 shows the variations of spatially averaged ($-3 \le z/D \le 3$: $0 \le x/D \le 20$) film-cooling effectiveness for a cylindrical (L/D=6) and laidback fan shaped hole ($\alpha=30^o$, $\beta=14^o$, $\gamma=15^o$, and L/D=6.0) with the blowing ratio. As shown in this figure, even though the numerical results shows some quantitative discrepancies on the spatially averaged film-cooling effectiveness, the tendency with the blowing ratio show good agreement compared to the experimental data. Therefore, it can be seen that the accuracy of the present numerical analysis is acceptable for the optimization.

Since the film-cooling techniques uses bleed air from the compressor, the use of more coolant causes reduction of overall engine efficiency. That is, the goal of film-cooling is to obtain high cooling efficiency by using less amount of coolant. Therefore, the present optimization is performed at low blowing ratio (M=0.5). The laidback fan shaped film-cooling hole is optimized in terms of four design variables, α, β, γ, and L/D. The design space, which is determined by the lower and upper limits of the variables, is shown in Table 1. The objective functions which are defined as the spatially averaged film-cooling effectiveness and the aerodynamic loss are numerically evaluated through RANS analysis at 35 experimental points that are selected through the

**Table 2** Comparison of the predicted and RANS calculated values at the optimal designs

| Shapes | Design variables | | | | Predicted value by hybrid MOEA | | RANS calculated value | |
|---|---|---|---|---|---|---|---|---|
| | α ($^o$) | β ($^o$) | γ ($^o$) | L/D | $F_{FCE}$ | $F_{AL}$ | $F_{FCE}$ | $F_{AL}$ |
| Opt. A | 49.02 | 19.58 | 10.45 | 7.933 | 5.268 | 0.034 | 5.285 | 0.036 |
| Opt. B | 40.14 | 15.89 | 4.719 | 7.132 | 5.523 | 0.027 | 5.581 | 0.029 |
| Opt. C | 36.66 | 12.14 | 2.666 | 6.992 | 5.959 | 0.024 | 6.142 | 0.026 |

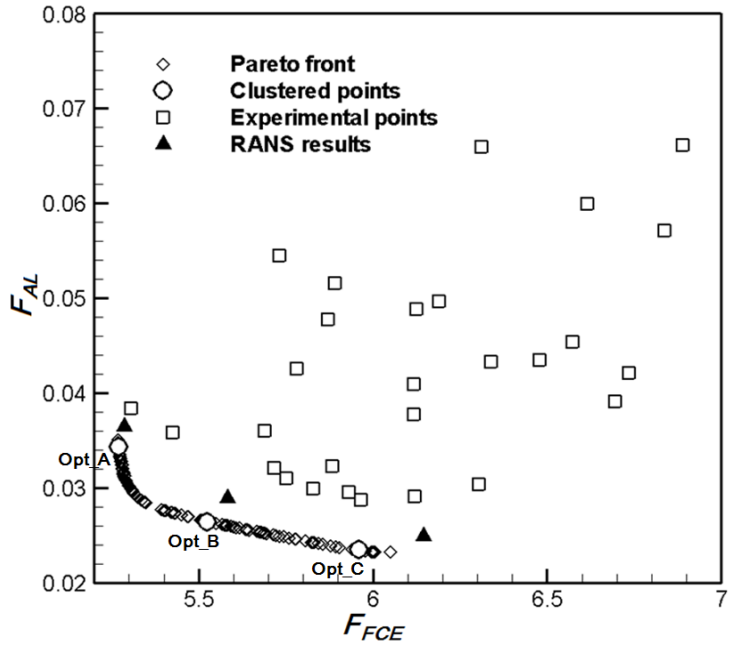


**Fig. 7** MOEA predictions and corresponding results from RANS analysis

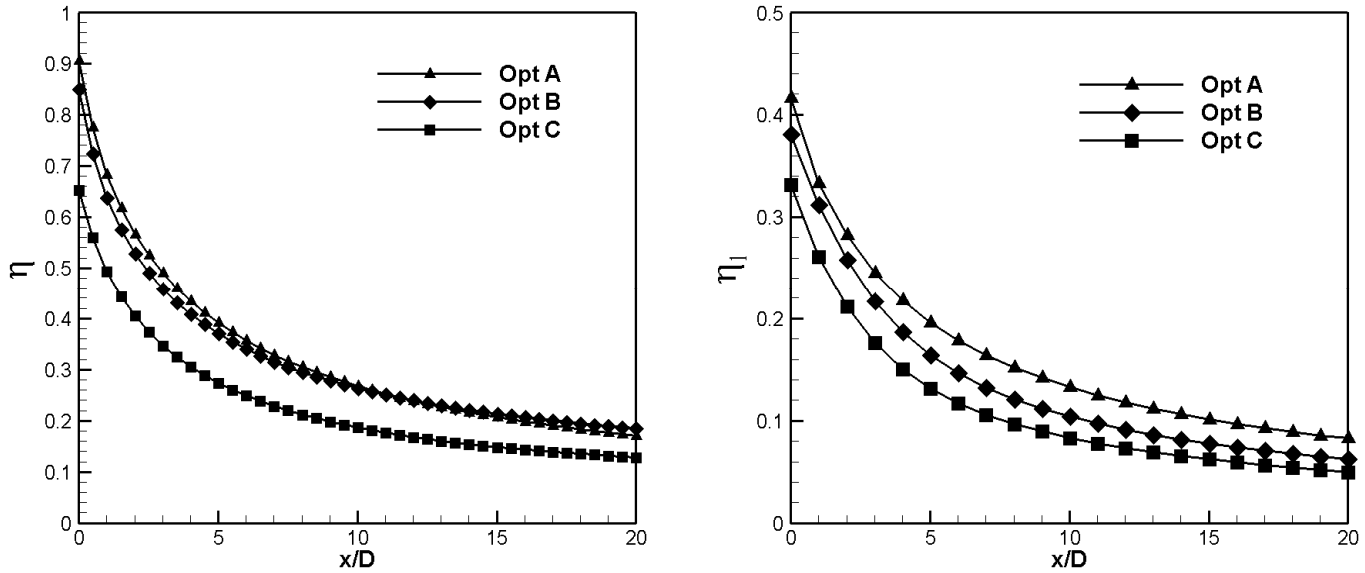


(a) Centerline film-cooling effectiveness (b) Laterally averaged film-cooling effectiveness

**Fig. 8** Comparison with the film-cooling effectiveness for the optimum designs

LHS. Using these data, RSA model is constructed, and the global Pareto optimal solutions by hybrid MOEA.

If the design variables, α, β, γ and L/D are represented by $x_1$, $x_2$, $x_3$ and $x_4$, the functional form of the objectives that are obtained by RSA can be expressed,:

$$F_{FCE} = 7.305 - 3.789x_1 - 1.819x_2 + 2.028x_3 - 0.233x_4 + 1.054x_1x_2 - 6.892x_1x_3 - 2.892x_1x_4 - 0.859x_2x_3 - 0.048x_2x_4 + 1.079x_3x_4 + 4.924x_1^2 + 1.033x_2^2 + 3.905x_3^2 + 1.251x_4^2 \quad (15)$$

$$F_{AL} = 0.049 - 0.058x_1 + 0.032x_2 + 0.015x_3 - 0.038x_4 - 0.039x_1x_2 - 0.097x_1x_3 - 0.038x_1x_4 + 0.015x_2x_3 - 0.003x_2x_4 + 0.031x_3x_4 + 0.093x_1^2 - 0.002x_2^2 + 0.055x_3^2 + 0.041x_4^2 \quad (16)$$

These equations are used as input function of NSGA-II and Pareto optimal front is produced.

Pareto optimal font (POF) is shown in Fig. 6, and the curve represents all the optimal designs generated by hybrid MOEA. The three cluster points from the hybrid MOEA are plotted and these selected optimal designs (Opt. A, Opt. B and Opt. C) are evaluated by RANS analysis. The Opt. A represents the high film-cooling effectiveness and high aerodynamic loss. On the other hand, the Opt. C shows the low film-cooling effectiveness and low aerodynamic loss. Hence, the designers can select any optimum design from the POF according to their needs.

Table 2 shows the optimal designs clustered from POF and their objective function values, and Fig. 7 shows the objective

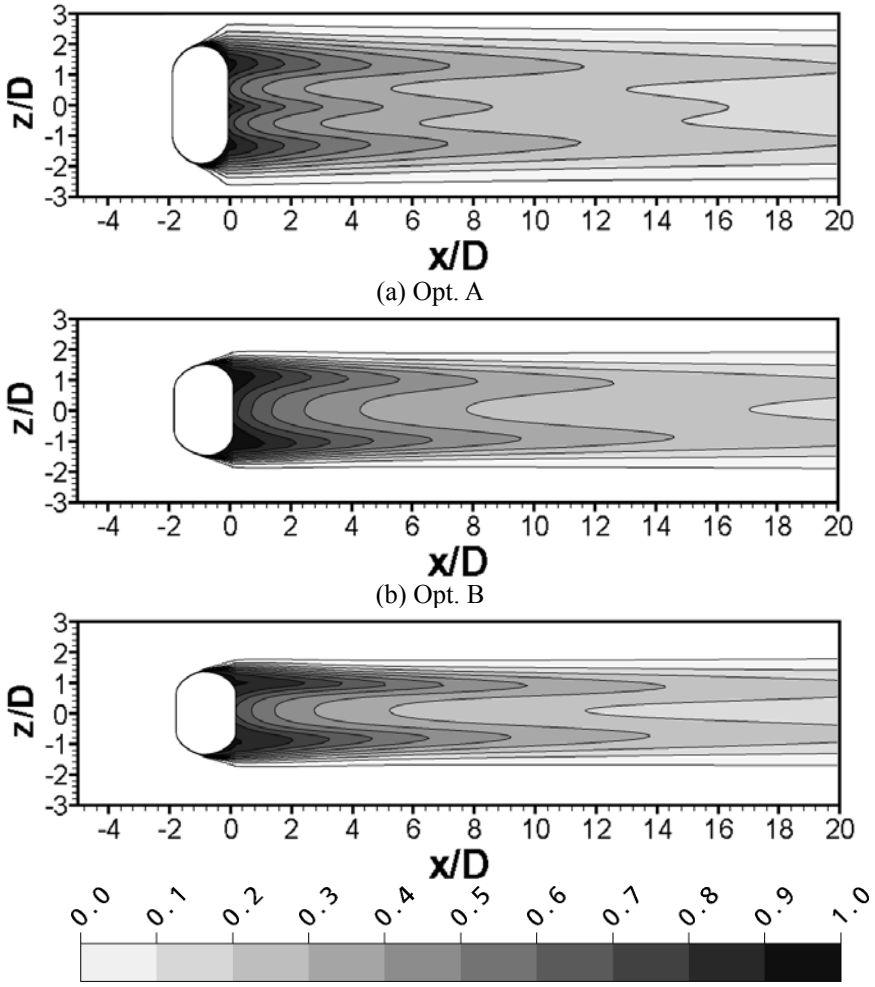


(a) Opt. A

(b) Opt. B

(c) Opt. C

**Fig. 9** Local film-cooling effectiveness distributions on the cooling surface

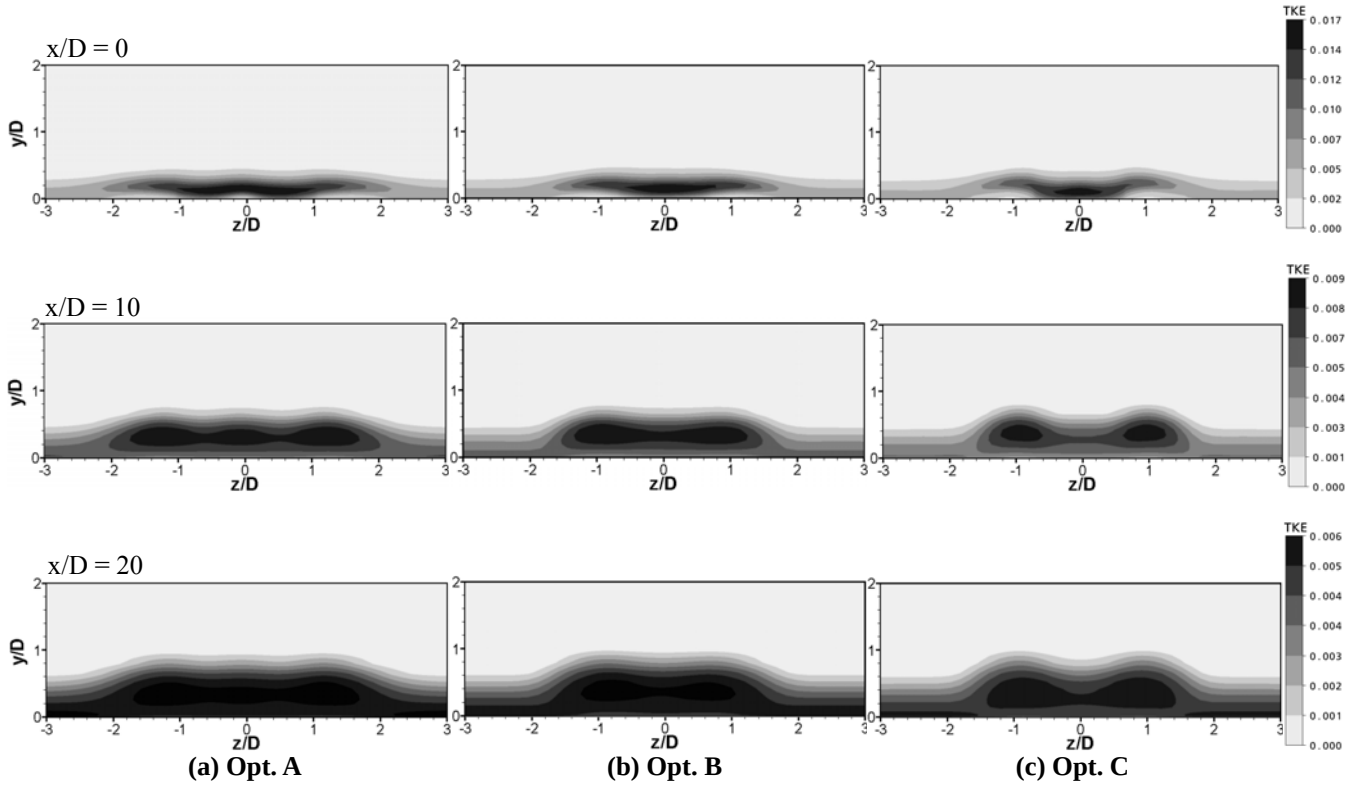


**(a) Opt. A** **(b) Opt. B** **(c) Opt. C**

**Fig. 10** Turbulence kinetic energy ($K/U_\infty$) distribution on y-z plane

function values for the experimental designs and the optimum designs obtained by RANS analysis. From these results, it is noted that the increased design variable values (α, β, γ and L/D) produce the high spatially averaged film-cooling effectiveness and high aerodynamic loss. Although the objective function values obtained by RANS analysis show some differences (0.3% ~ 8.3%) with the predicted values, the tendency of the objective functions with the design variables shows good agreement with the POF. And, in comparison with the all experimental designs, the optimum designs give enhanced objective function values.

The centerline and laterally averaged film-cooling effectiveness distributions along the streamwise direction for the optimum designs are graphically shown in Fig. 8. The Opt. A shows the film-cooling effectiveness distributions that are larger than those of the Opt. B and C through the downstream region of the film-cooling hole.

Fig. 9 shows the local film-cooling effectiveness distributions on the film-cooling surface for the optimum designs. Diffused exit shaped hole generally yield the typical bimodal pattern of the local film-cooling effectiveness that is caused by the separation inside the diffuser [3] as seen in Opt. B and C. However, Opt. A shows the three-forked distribution of film-cooling effectiveness that makes higher film-cooling effectiveness. And enhanced lateral spreading also contribute the increase of spatially averaged film-cooling effectiveness.

Fig. 10 represents the normalized turbulence kinetic energy ($K/U_\infty$) distributions on y-z plane at x/D=0, 10 and 20. For the Opt. A, relatively higher turbulence intensity is generated in the wider region which causes higher aerodynamic loss.

## 6. Conclusions

A laidback fan shaped film-cooling hole has been formulated numerically and optimized using RANS analysis and hybrid multi-objective evolutionary algorithm. The computational results with low-Re SST turbulence model for film-cooling effectiveness show good agreement with the experimental data. The design optimization of film-cooling hole has been performed to enhance the film-cooling effectiveness compromising the aerodynamic loss with four design variables, viz., the injection angle of the hole, the lateral expansion angle of the diffuser, the forward expansion angle of the hole, and the ratio of the length to diameter of the hole. The objective functions have been calculated at the design points selected by using LHS method. Both film-cooling effectiveness and aerodynamic loss based objectives are optimized, and a set of optimum designs have been presented by POF. Three optimum designs from POF have been selected and analyzed by flow analysis. The increased design variable values (α, β, γ and L/D) produced the high spatially averaged film-cooling effectiveness as well as high aerodynamic loss. And, the optimum designs show enhanced objective function values as compared with the experimental designs.

## Acknowledgments

This work was supported by the National Research Foundation of Korea (NRF) grant No. 2009-0083510 funded by the Korean government (MEST) through Multi-phenomena CFD Engineering Research Center.

## Nomenclature

| | | | |
|---|---|---|---|
| D | Film-cooling hole diameter | $y+$ | y in law of the wall coordinate |
| $F_{AL}$ | Objective function for film-cooling effectiveness | α | injection angle of hole |
| $F_{FCE}$ | Objective function for aerodynamic loss | β | lateral expansion angle of cooling hole diffuser |
| L | Film-cooling hole length | γ | forward expansion angle of cooling hole diffuser |
| M | Bowing ratio $(=\rho_2 U_2)/(\rho_\infty U_\infty)$ | $\rho_2$ | density of coolant |
| $T_{aw}$ | Adiabatic wall temperature | $\rho_\infty$ | density of hot gas |
| $T_\infty$ | Free stream temperature in main channel | $\eta$ | film-cooling effectiveness: $(T_{aw}-T_\infty)/(T_c-T_\infty)$ |
| $T_c$ | Coolant jet temperature | $\eta_l$ | laterally averaged film-cooling effectiveness ($-3\le z/D\le 3$) |
| $U_2$ | Velocity of coolant at hole exit | | |
| $U_\infty$ | Velocity at the inlet of hot gas | $\eta_s$ | spatially averaged film-cooling effectiveness ($-3\le z/D\le 3$: $0\le x/D\le 20$) |
| $y$ | Distance from the wall | | |

## References

[1] Goldstein, R. J., Eckert, E. R. G., and Burggraf, F., 1974, "Effects of Hole Geometry and Density on Three-Dimensional Film Cooling," Int. J. Heat Mass Transfer, Vol. 17, pp. 595-607.

[2] Gritsch, M., Schulz, A., and Wittig, S., 1998, "Adiabatic Wall Effectiveness Measurements of Film-Cooling Holes With Expanded Exits," ASME J. Turbomachinery, Vol. 120, pp. 549-556.

[3] Saumweber, C. and Schulz, A., 2008, "Effect of Geometry Variations on the Cooling Performance of Fan-Shaped Cooling Holes," ASME Turbo Expo 2008, Berlin, GT2008-51038.

[4] Saumweber, C., Schulz, A., and Wittig, S., 2003, "Free-stream Turbulence Effects on Film Cooling With Shaped Holes," ASME J. Turbomachinery, Vol. 125, pp. 65-73.

[5] Lutum, E. and Johnson, B. V., 1999, "Influence of the Hole Length-to-Diameter Ratio on Film Cooling With Cylindrical Holes," ASME J. Turbomachinery, Vol. 121, pp. 209-216.

[6] Bunker, R. S., 2005, "A Review of Shaped Hole Turbine Film-Cooling Technology," J. Heat Transfer, Vol. 127, pp. 441-453.

[7] Bohn, D. and Moritz, N., 2003, "Numerical Parametric Study on Full Coverage Cooled Multi-Layer Plates," Proceeding of the International Gas Turbine Congress 2003, Tokyo, IGTC2003 Tokyo TS-84.

[8] Hyams, D., G. and Leylek, J. H., 2000, "A Detailed Analysis of Film Cooling Physics: Part3-Streamwise Injection With Shaped Holes," ASME J. Turbomachinery, Vol. 122, pp. 122-132.

[9] Azzi, A. and Jubran, B. A., 2007, “Numerical modeling of film cooling from converging slot-hole,” Heat Mass Transfer, Vol. 43, pp. 381-388.
[10] Leedom, D. H. and Acharya, S., 2008, “Large Eddy Simulation of Film Cooling Flow Field From Cylindrical and Shaped Holes,” ASME Turbo Expo 2008, Berlin, GT2008-51009.
[11] Mahmood, S., Kassab, A. J., and Divo, E., 2005, “Film Cooling Effectiveness from a Single Scaled-Up Fan-Shaped Hole: A CFD Simulation of Adiabatic and Conjugate Heat Transfer Models,” ASME Turbo Expo 2005, Nevada, GT2005-68431.
[12] Day, C. R. B., Oldfield, M. L. G., and Lock, G. D., 2000, “Aerodynamic performance of an annular cascade of film cooled nozzle guide vanes under engine representative conditions,” Experiments in Fluids, Vol. 29, pp. 117-129.
[13] Sargison, J. E., Guo, S. M., Oldfield, M. L. G., Lock, G. D., and Rawlinson, A. J., 2002, “A Converging Slot-Hole Film-Cooling Geometry-Part 1: Low-Speed Flat-Plate Heat Transfer and Loss,” ASME J. Turbomachinery, Vol. 124, pp. 453-460.
[14] Walters, D. K. and Leylek, J. H., 2000, “Impact of Film-Cooling Jets on Turbine Aerodynamic Losses,” ASME J. Turbomachinery, Vol. 122, pp. 537-545.
[15] Lee, K. D. and Kim, K. Y., 2009, “Optimization of a Cylindrical Film Cooling Hole using Surrogate Modeling,” Numerical Heat Transfer A, Vol. 55, No. 4, pp. 362-380.
[16] Lee, K. D. and Kim, K. Y., 2010, “Shape optimization of a fan-shaped hole to enhance film-cooling effectiveness,” Int. J. Heat and Mass Transfer, Vol. 53, pp. 2996-3005.
[17] Deb, K., 2001, Multi-objective optimization using evolutionary algorithms, Wiley, New York.
[18] Marler, R. T. and Arora, J. S., 2004, “Survey of multi-objective optimization methods for engineering,” Struct. Multidisciplinary Opt., Vol. 26, No. 6, pp. 369-395.
[19] Samad, A., Lee, K. D., and Kim, K. Y., 2008, “Multi-objective optimization of a dimpled channel for heat transfer augmentation,” Heat Mass Transfer, Vol. 45, pp. 207-217.
[20] Foil, K., Okabe, T., Olhofer, M., Jin, Y., and Sendhoff, B., 2006, “Optimization of micro heat exchanger: CFD, analytical approach and multi-objective evolutionary algorithms,” Int. J. Heat and Mass Transfer, Vol. 49, pp. 1090-1099.
[21] Samad, A. and Kim, K. Y., 2009, “Surrogate Based optimization Techniques for Aerodynamic Design of Turbomachinery,” Int. J. Fluid Machinery and Systems, Vol. 2, No. 2, pp. 179-188.
[22] CFX-11.0 Solver Theory, Ansys inc., 2008.
[23] Menter, F. and Esch, T., 2001, “Elements of Industrial Heat Transfer Prediction,” 16th Brazilian Congress of Mechnacal Engineering (COBEM), Uberlandia Brazil.
[24] Bardina, J. E., Huang, P. G., and Coakley, T., 1997, “Turbulence Modeling Validation,” Fluid Dynamics Conference 28th, AIAA Paper 1997-2121.
[25] Myers, R. H. and Montgomery, D. C., 1995, Response surface methodology-process and product optimization using designed experiments, Wiley, New York.
[26] MATLAB, The language of technical computing, Release 14, The math Works Inc.